

Fine-Grained Instruction-Guided Graph Reasoning for Vision-and-Language Navigation

Yaohua Liu*, Xinyuan Song*, Yunfu Deng, Yifan Xie, Binkai Ou, Yan Zhong†

Abstract—Vision-and-Language Navigation (VLN) requires an embodied agent to traverse complex environments by following natural language instructions, demanding accurate alignment between visual observations and linguistic guidance. Despite recent progress, existing methods typically encode visual and directional cues in a coupled manner, and process instructions without explicitly extracting navigation-critical semantics, which often leads to imprecise spatial reasoning and suboptimal cross-modal alignment. To address these challenges, we propose a fine-grained instruction-guided graph reasoning framework (OIKG) that enhances both spatial representation and instruction understanding during navigation. Specifically, an observation-graph interaction mechanism is introduced to disentangle angular and visual cues while strengthening directed edge representations through geometric embedding, enabling more reliable spatial reasoning within the navigation graph. In addition, a fine-grained instruction guidance module is designed to explicitly extract and leverage location-specific and object-centric information from language instructions, facilitating more precise cross-modal alignment between linguistic semantics and navigable trajectories. By jointly integrating structured graph reasoning with instruction-critical semantic cues, the proposed approach significantly improves the agent’s ability to follow complex navigation instructions. Extensive experiments on the R2R and RxR benchmarks demonstrate that our method consistently achieves state-of-the-art performance across multiple evaluation metrics, validating the effectiveness of fine-grained instruction-guided graph reasoning for vision-and-language navigation.

Index Terms—Vision-and-language navigation, cross-modal alignment, graph reasoning, spatial representation learning.

I. INTRODUCTION

VISION-and-Language Navigation (VLN) [1]–[7] is a challenging embodied intelligence task that requires an agent to navigate within complex three-dimensional environments [8], [9] by executing natural language instructions. Successful navigation depends on the agent’s ability to jointly interpret visual observations of its surroundings and linguistic descriptions that specify spatial relations, landmarks, and target locations. This process involves reasoning over scene

geometry, recognizing objects and structural cues, and making sequential decisions guided by the alignment between visual perception and instruction semantics. Unlike purely vision-based navigation, VLN demands robust cross-modal understanding, where subtle discrepancies between observation and language can accumulate over time and lead to navigation failure, particularly in long-horizon and instruction-dense scenarios [10]–[12]. Consequently, effective integration of visual representations and fine-grained linguistic guidance is central to achieving accurate and reliable navigation behavior in VLN tasks.

Recent advances [13]–[18] in Vision-and-Language Navigation have increasingly leveraged explicit spatial representations to improve long-horizon decision making. In particular, a line of work introduces topological graph structures that record explored viewpoints and their connectivity, enabling agents to reason beyond purely local observations. Within such graph-based formulations, each node typically corresponds to a navigable viewpoint, while edges encode spatial transitions, allowing information to be propagated across the navigation space using graph neural networks or transformer-based encoders. This paradigm supports more strategic planning by aggregating visual context and linguistic guidance over previously visited locations. For example, DUET [13] combines global graph-level encoding with fine-grained local observation modeling to balance long-term planning and immediate action selection, while BEVBert [17] integrates local metric representations with global topological maps to enhance spatial awareness and cross-modal reasoning. More recently, PRET [18] proposes a directed graph formulation that incorporates orientation-aware features into trajectory planning, offering an alternative to conventional undirected graph encoding and enabling more structured navigation decisions.

Despite the substantial progress achieved by graph-based VLN methods, several fundamental challenges remain unresolved. A primary limitation lies in the way visual observations [19]–[22] and angular information are commonly represented: many existing approaches encode these heterogeneous cues within a single feature space, despite their distinct semantic roles in navigation. Such entangled representations may introduce interference between directional reasoning and visual perception, thereby reducing the precision of spatial decision making. In addition, navigation instructions [23]–[26] are often treated as holistic textual inputs and integrated into the navigation process through generic attention mechanisms. This coarse-grained strategy fails to explicitly capture instruction-critical elements, such as location descriptors and object references, which are essential for resolving where

* Equal Contribution. †Corresponding author.

Y. Liu is with Guangdong Institute of Intelligence Science and Technology, Hengqin, Zhuhai, Guangdong, China, 519031 (e-mail: liuyaohua@gdiist.cn).

X. Song is with the Department of Computer Science, Emory University, USA.

Y. Deng is with the Department of Computer Science, University of Wisconsin-Madison, USA.

Y. Xie is with Tsinghua University and Guangdong Institute of Intelligence Science and Technology, China.

B. Ou is with the Innovation and Research and Development Department, BoardWare Information System Company and Guangdong Institute of Intelligence Science and Technology, China.

Y. Zhong is with the School of Mathematics, Peking University, China (e-mail: zhongyan@stu.pku.edu.cn).

the agent should move and what it should attend to at each step. As a result, current methods may struggle to maintain consistent instruction-following behavior, particularly in complex environments with long trajectories and densely specified instructions.

To address the aforementioned limitations, we propose a new framework for Vision-and-Language Navigation based on fine-grained instruction-guided graph reasoning (OIKG). The proposed approach introduces two complementary design principles. First, an observation-graph interaction mechanism is developed to decouple angular cues from visual representations while explicitly enhancing directed edge modeling through geometric embedding, thereby improving spatial reasoning within the navigation graph. Second, a fine-grained instruction guidance module is designed to selectively extract location-specific and object-centric semantic cues from natural language instructions and to incorporate these cues into the graph reasoning process, enabling more precise alignment between linguistic guidance and navigable trajectories. By jointly strengthening spatial representation and instruction-level semantic modeling, the proposed framework facilitates more accurate navigation decisions and improved trajectory consistency. To assess the effectiveness of the proposed OIKG framework, we conduct comprehensive experiments on the R2R and RxR benchmarks. The experimental results consistently show that OIKG outperforms existing approaches across multiple evaluation metrics.

This article is an extended version of our prior conference paper [27]. Compared with the conference version, this journal extension includes more detailed theoretical derivations and a deeper analysis of experimental results, providing a clearer understanding of the proposed method and its empirical behavior across different navigation settings.

The main contributions of this work can be summarized as follows:

- 1) We propose a fine-grained instruction-guided graph reasoning framework for Vision-and-Language Navigation that jointly enhances spatial reasoning and instruction-level semantic alignment.
- 2) We introduce an observation-graph interaction mechanism that decouples angular and visual information while strengthening directed edge representations through geometric embedding.
- 3) We design a fine-grained instruction guidance module that explicitly extracts and exploits location-specific and object-centric semantic cues from navigation instructions for improved cross-modal alignment.
- 4) We provide a theoretical analysis that explains how the proposed design reduces representational interference and improves optimization stability and semantic alignment.
- 5) We conduct extensive experiments on the R2R and RxR benchmarks, demonstrating consistent performance improvements over existing state-of-the-art methods.

The rest of this paper is organized as follows. Section II reviews related work on Vision-and-Language Navigation and graph-based spatial representations. Section III describes the proposed fine-grained instruction-guided graph reasoning

framework in detail. Section IV presents the theoretical analysis of the proposed method. Section V reports experimental results and ablation studies. Finally, Section VI concludes the paper and discusses future research directions.

II. RELATED WORKS

A. Vision-and-Language Navigation

VLN [13]–[18], [28]–[30] has attracted increasing attention in recent years as a core problem in embodied artificial intelligence, where agents are required to execute natural language instructions in visually rich environments. Early VLN approaches predominantly relied on sequence-to-sequence architectures based on recurrent neural networks, mapping textual instructions to either low-level navigation actions or high-level waypoint decisions using discretized panoramic visual observations. While effective in simple scenarios, these methods often suffered from limited generalization and insufficient long-horizon reasoning capability.

To alleviate data scarcity and improve robustness, subsequent studies introduced various data augmentation techniques including back-translation [28] and environment-level dropout [31]–[33]. Attention-based mechanisms [34]–[36] were also explored to enhance cross-modal alignment during navigation.

With the emergence of transformer architectures, recent VLN research has shifted toward more expressive representation learning and planning strategies. PREVALENT [37] pioneers large-scale pretraining for VLN by initializing transformer encoders on navigation-related data, significantly improving generalization to unseen environments. MTVM [38] further extends this direction by incorporating navigation history memorization within a transformer framework, allowing agents to reason over variable-length trajectories and develop more robust planning behaviors.

Beyond representation learning, navigation strategy design has become a central focus, particularly for improving exploration and decision making in unseen environments. DUET [13] introduces a dual-scale transformer architecture that jointly models local observations and global topological context, enabling balanced short-term action selection and long-term planning. AZHP [14] proposes a hierarchical graph structure to improve exploration efficiency, while Meta-Explore [15] explicitly models backtracking decisions to enhance trajectory recovery. BEVBert [17] integrates local metric maps with global topological graphs, strengthening spatial understanding through hybrid mapping representations. More recently, PRET [18] formulates VLN planning using directed graph structures with orientation-aware trajectory encoding, offering an alternative to conventional graph convolution-based map representations and enabling more structured navigation reasoning. In contrast to these methods, our work builds upon directed graph formulations and addresses two underexplored aspects: (1) decoupling angular and visual cues within graph representations, and (2) explicitly extracting navigation-critical semantics from instructions for tighter cross-modal alignment.

B. Maps for Navigation

Spatial mapping has long been a central component of visual navigation systems, with early research primarily grounded in simultaneous localization and mapping (SLAM) techniques [39], [40]. Classical approaches construct metric maps encoding geometric layouts [41]–[43], enabling precise localization but often incurring substantial computational overhead that limits scalability.

To improve efficiency, subsequent studies explored topological map representations [44], [45], where environments are modeled as graphs composed of discrete nodes and navigable connections. Compared to dense metric maps, topological graphs offer a more compact and computationally efficient abstraction for global planning, albeit at the cost of reduced local geometric precision. This trade-off motivated the development of hybrid mapping strategies that combine metric and topological representations, aiming to exploit detailed local geometry while retaining efficient long-range reasoning.

Recent advances [13], [17], [46] have further introduced learnable mapping frameworks that integrate spatial representations into end-to-end navigation models. For example, several works incorporate neural metric maps for short-term spatial reasoning while maintaining global topological graphs to support long-horizon planning. BEVBert [17] exemplifies this direction by jointly learning local metric and global topological representations. However, processing hybrid maps often remains computationally demanding, particularly when dense metric representations are repeatedly updated during navigation.

To address these challenges, alternative formulations [18], [45] have investigated graph-centric navigation strategies that avoid explicit metric map construction. Directed topological maps and trajectory-based planning methods enable incremental embedding updates and reduce computational complexity while preserving effective spatial reasoning capabilities. By encoding orientation-aware transitions and trajectory fidelity within directed graphs, these approaches support structured planning without relying on dense geometric maps. Building on this line of work, our method adopts a directed graph formulation and further enhances edge representations through observation–graph interaction, enabling more accurate and efficient spatial reasoning for vision-and-language navigation.

III. METHOD

A. Problem Statement

VNL [8], [9], [13] is formulated in a discrete environment [47] represented by a navigation graph $G = \{\mathcal{V}, \mathcal{E}\}$, where $\mathcal{V} = \{V_i\}_{i=1}^N$ denotes the set of navigable nodes and \mathcal{E} represents the traversable connections between nodes. An agent is initialized at a starting node and is provided with a natural language instruction $I = \{I_i\}_{i=1}^M$ consisting of M words, which specifies the target destination through spatial and semantic descriptions. The objective of the agent is to follow the instruction and navigate through the graph to reach the target location.

At each time step t , the agent located at node V_t perceives its surroundings through a 360-degree panoramic observation

$O_t = \{r_{t,i}\}_{i=1}^K$, where each $r_{t,i}$ corresponds to the visual feature extracted from the i -th viewpoint. The agent also has access to a set of navigable neighboring nodes $\mathcal{N}(V_t) \subset \mathcal{V}$, along with their relative spatial coordinates and orientations with respect to the current position. Based on the observed visual information, spatial geometry, and linguistic guidance, the agent must decide whether to transition to one of the neighboring nodes or remain at its current location.

Navigation is considered successful when the agent terminates within a predefined Euclidean distance threshold (3 meters) from the target position. The task therefore requires the agent to balance perception, language understanding, and sequential decision making over a finite horizon T , while maintaining consistent cross-modal alignment between visual observations and instruction semantics throughout the navigation process.

B. Model Overview

Fig. 1 presents an overview of the proposed fine-grained instruction-guided graph reasoning framework. At each time step t , the agent receives a panoramic visual observation O_t , from which observation features F_o are extracted using a pretrained visual encoder [20]. In parallel, a navigation graph $G_t = \{\mathcal{V}_t, \mathcal{E}_t\}$ is maintained to represent the agent’s explored environment, where nodes correspond to navigable viewpoints and directed edges encode orientation-aware transitions. Unlike prior approaches [13], [17] that directly assign panoramic features to visited nodes and directional views to unvisited nodes, leading to inconsistent representations, we adopt a directed graph formulation that incrementally incorporates nodes and edges as navigation proceeds. This design ensures a unified and consistent representation for both visited and candidate nodes.

The navigation graph features F_g are constructed from directed edges that capture both visual observations and angular information associated with specific movement directions. Since observation and graph features inherently contain heterogeneous cues, including visual appearance and orientation, directly fusing them may introduce representational interference. To address this issue, we introduce an observation–graph interaction mechanism (Sec. III-C) that explicitly decouples angular and visual information within observation features. The angular cues derived from panoramic observations are further integrated into the graph representation through geometric embedding, strengthening the expressiveness of directed edges and enabling more accurate spatial reasoning. Based on this interaction, candidate node features are iteratively updated, resulting in an enhanced graph representation G'_t .

Given the updated graph G'_t , the navigation instruction I is incorporated to guide action selection. Specifically, the graph features are fused with instruction features through a multi-layer transformer decoder to obtain cross-modal representations that encode the alignment between linguistic semantics and navigable trajectories. To further improve instruction utilization, we introduce a fine-grained instruction guidance module that dynamically extracts instruction-critical semantic cues, including location-specific and object-centric

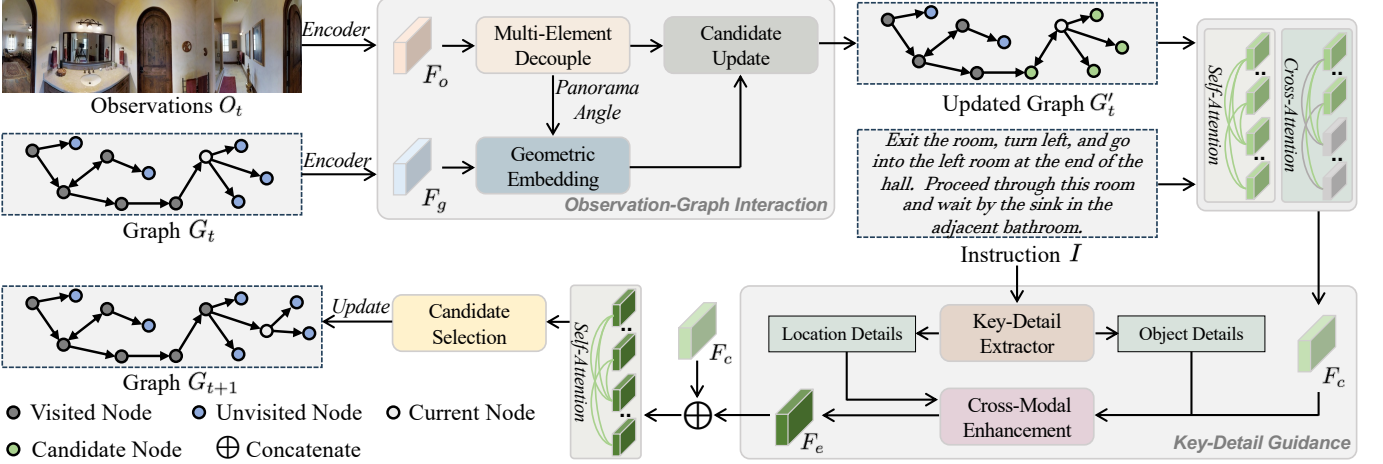


Fig. 1. Illustration of our proposed OIKG architecture. At time step t , given the observation O_t and the path graph G_t , the observation features F_o and graph features F_g are extracted respectively, where the Observation-Graph Interaction module is employed to strengthen the edge representation and update the candidate nodes. Then, we design the Key-Detail Guidance module to further extract the detailed information from the text instruction I , and enhance the alignment between instruction and navigation path. Finally, a Candidate Selection module updates the path graph G_{t+1} for the next step.

information. These cues are used to enhance cross-modal representations via a dedicated interaction mechanism, producing instruction-aware features that emphasize decision-relevant information.

Finally, a candidate selection module predicts the next navigation action by scoring candidate nodes based on their alignment with the enhanced instruction-aware features. The selected node is used to update the navigation graph G_{t+1} , and the process is repeated until the agent terminates or reaches the maximum time step. Through the integration of observation-graph interaction and fine-grained instruction guidance, the proposed framework enables consistent spatial reasoning and precise instruction following throughout the navigation process.

C. Observation-Graph Interaction

Given the observation features F_o and graph features F_g , we introduce an observation-graph interaction mechanism to enhance directed edge representations and iteratively update candidate node features. The observation features extracted from panoramic views inherently contain heterogeneous information, including visual appearance and angular cues. Treating these components as a unified representation may lead to mutual interference, as angular information primarily supports directional reasoning, whereas visual features encode semantic and appearance-related cues. To mitigate this issue, we explicitly decouple the observation features into angular and visual components and process them separately.

Specifically, the angular and visual components are independently embedded to obtain angular embeddings E_a and visual embeddings E_v , respectively. These embeddings are then concatenated and fused through a multilayer perceptron to form the refined observation representation:

$$F'_o = \mathcal{F}(\text{cat}[E_a, E_v]), \quad (1)$$

where $\text{cat}[\cdot]$ denotes the concatenation and $\mathcal{F}(\cdot)$ represents the fusion function implemented by an MLP. This decoupling

and-fusion strategy reduces representational interference while preserving complementary information from both modalities.

For graph features, we focus on angular information to model directional perception, as orientation plays a dominant role in navigation decisions. The angular representation consists of both heading and elevation angles, where heading information is emphasized due to its greater influence on horizontal navigation. For each candidate node, we extract the sine and cosine representations of the heading angle α , denoted as $\sin(\alpha)$ and $\cos(\alpha)$. Correspondingly, we obtain the angular representations $\sin(\alpha')$ and $\cos(\alpha')$ from the observation features. The relative angular difference is computed using a trigonometric formulation:

$$d = |(\text{atan2}[\sin(\alpha - \alpha'), \cos(\alpha - \alpha')])|. \quad (2)$$

Based on the relative angular differences, we identify the closest angular distance d' for each candidate view and construct a geometric positional embedding:

$$pe = \mathcal{P}(\text{cat}[d', \sin(\alpha - \alpha'), \cos(\alpha - \alpha')]), \quad (3)$$

where $\mathcal{P}(\cdot)$ denotes a linear projection function. This positional embedding encodes the spatial relationship between candidate nodes and the current observation, enabling the model to distinguish candidate directions more effectively.

The final candidate node features are obtained by combining the raw angular information with the positional embedding through element-wise addition:

$$F'_g = \mathcal{C}(\text{cat}[\sin(\alpha), \cos(\alpha), \sin(\beta), \cos(\beta)]) + pe, \quad (4)$$

where β denotes the elevation angle and $\mathcal{C}(\cdot)$ is a linear transformation. This formulation enriches the graph representation with explicit geometric priors while maintaining a compact feature structure.

To update directed edge features and incorporate observation-level context, we employ a transformer decoder layer [34] for observation-graph interaction. In this process,

Instruction	Location
Exit the bedroom , go passed the table with china on it, turn left into the doorway , and then turn right , go straight passed the china case and then turn left into the doorway . Step between the bed and the window on the right and stop.	bedroom right between
	Object
	table bed china china case window

Fig. 2. The process of extracting location and object details from the original instruction.

candidate node features serve as queries, while the refined observation features F'_o act as keys and values. This attention-based interaction allows each directed edge to selectively attend to observation regions corresponding to its spatial orientation, resulting in an updated navigation graph G'_t with strengthened edge representations and improved directional consistency.

D. Key-Detail Guidance

After obtaining the updated navigation graph G'_t , the natural language instruction I is incorporated to guide the agent’s navigation decisions. We first fuse the graph representation with instruction features using a multi-layer transformer decoder, producing cross-modal features F_c that encode interactions between navigable trajectories and linguistic semantics. While such cross-attention mechanisms [34] are effective for coarse alignment, they often treat the instruction as a holistic input and may include redundant or decision-irrelevant information, limiting their ability to provide precise step-wise guidance.

To address this limitation, we introduce a key-detail guidance module that explicitly models fine-grained semantic cues within navigation instructions. Specifically, we categorize instruction-critical information into two complementary types [13], [17], [18], [48]: location-specific cues (e.g., room types or spatial regions) and object-centric cues (e.g., landmarks or reference objects). Using a large language model, we preprocess the instruction corpus to identify and organize location and object vocabularies. Based on these vocabularies, the corresponding token-level features are extracted from the instruction representation produced by a multi-layer transformer encoder initialized with pretrained language models.

The extracted location and object features are independently projected and fused to form the key-detail feature representation:

$$F_k = \mathcal{F}'(\text{cat}[\mathcal{E}_{\mathcal{L}}(F_i), \mathcal{E}_{\mathcal{O}}(F_i)]), \quad (5)$$

where F_i denotes the instruction features, $\mathcal{E}_{\mathcal{L}}(\cdot)$ and $\mathcal{E}_{\mathcal{O}}(\cdot)$ are linear projection layers for location and object details, respectively, and $\mathcal{F}'(\cdot)$ represents the key-detail fusion function. This representation explicitly isolates instruction elements that are most relevant for navigation decisions.

To integrate key-detail information into the navigation process, we employ a cross-modal enhancement module consisting of a cross-attention mechanism followed by a linear projection. In this module, the cross-modal features F_c serve as queries, while the key-detail features F_k act as keys and values. This design enables the model to selectively emphasize instruction-critical semantics when reasoning about candidate

trajectories. The resulting enhanced features F_e capture fine-grained alignment between navigable paths and instruction details, with particular sensitivity to spatial and object-related cues.

Finally, the enhanced features are combined with the original cross-modal features through a residual connection and further refined using a self-attention mechanism to model global dependencies across candidate nodes. An MLP is applied to compute alignment scores that measure the semantic compatibility between each candidate node and the navigation instruction. The next action a_t^p is selected by choosing the candidate with the highest alignment score, and the navigation graph is updated accordingly for the subsequent time step. Through explicit modeling of instruction-critical details, the proposed guidance mechanism improves decision precision and robustness in instruction-dense navigation scenarios.

E. Loss Function

Following common training paradigms [13], [17], [18], [37] in Vision-and-Language Navigation, we adopt a two-stage training strategy consisting of pretraining and task-specific fine-tuning. During the pretraining stage, Masked Language Modeling (MLM) is employed to initialize the model parameters. Specifically, 15% of the input tokens are randomly masked and fed into the text encoder. The encoded representations, together with the corresponding directed edge features, are processed by a transformer decoder to reconstruct the masked tokens. This pretraining objective encourages the model to learn robust cross-modal representations that effectively ground linguistic semantics in the navigation graph.

After pretraining, the model is fine-tuned using a hybrid learning strategy that combines teacher forcing and student forcing. In the teacher-forcing phase, the agent is guided by the ground-truth action sequence a_t^{gt} , while still conditioning on the model’s predicted actions a_t^p to maintain consistency between training and inference. In the student-forcing phase, pseudo actions a_t' are sampled from the model’s predicted action distribution to promote exploration and alleviate exposure bias.

For trajectories that deviate from the ground-truth path, we adopt a recovery strategy by assigning pseudo-labels based on the nearest unvisited ground-truth node. When no such nodes are available, pseudo-labels are determined using the shortest path between the current position and the target location. This mechanism enables the model to learn corrective behaviors when deviations occur.

The overall training objective is defined as a weighted combination of losses from teacher forcing and student forcing:

$$\mathcal{L} = \lambda \left(\frac{1}{T} \sum_{t=1}^T \eta(a_t^p, a_t^{gt}) \right) + (1 - \lambda) \left(\frac{1}{T} \sum_{t=1}^T \eta(a_t^p, a_t') \right), \quad (6)$$

where λ controls the balance between the two learning strategies, T denotes the total number of time steps, and $\eta(\cdot)$ represents the cross-entropy loss.

IV. THEORETICAL ANALYSIS

To further understand why the proposed OIKG framework improves navigation stability and decision accuracy, we now

TABLE I
EVALUATION RESULTS ON R2R DATASET UNDER DIFFERENT SETTINGS. BEST PERFORMANCE IS HIGHLIGHTED IN BOLD.

Methods	Val Seen				Val Unseen				Test Unseen			
	TL	NE↓	SR↑	SPL↑	TL	NE↓	SR↑	SPL↑	TL	NE↓	SR↑	SPL↑
Seq2Seq-SF [8]	11.33	6.01	39	-	8.39	7.81	22	-	8.13	7.85	28	18
Speaker-Follower [28]	-	3.36	66	-	-	6.62	35	-	14.82	6.62	35	28
RCM [29]	10.65	3.53	67	-	11.46	6.09	43	-	11.97	6.12	43	38
Regretful [49]	-	3.23	69	63	-	5.32	50	41	-	5.69	56	40
EnvDrop [31]	11.00	3.99	62	59	10.70	5.22	52	48	11.66	5.23	51	47
PREVALENT [37]	10.32	3.67	69	65	10.19	4.71	58	53	10.51	5.30	54	51
NvEM [50]	11.09	3.44	69	65	11.83	4.27	60	55	12.98	4.37	58	54
SSM [46]	14.70	3.10	71	62	20.70	4.32	62	45	20.40	4.57	61	46
RecBert [51]	11.13	2.90	72	68	12.01	3.93	63	57	12.35	4.09	63	57
HAMT [30]	11.15	2.51	76	72	11.46	2.29	66	61	12.27	3.93	65	60
MTVM [38]	-	2.67	74	69	-	3.73	66	59	-	3.85	65	59
DUET [13]	12.32	2.28	79	73	13.94	3.31	72	60	14.73	3.65	69	59
AZHP [14]	-	-	-	-	14.05	3.15	72	61	14.95	3.52	71	60
Meta-Explore [15]	11.95	2.11	81	75	13.09	3.22	72	62	14.25	3.57	71	61
GridMM [16]	-	-	-	-	13.27	2.83	75	64	14.43	3.35	73	62
BEVBert [17]	13.56	2.17	81	74	14.55	2.81	75	64	15.87	3.13	73	62
PRET [18]	11.25	2.41	78	72	11.87	2.90	74	65	12.21	3.09	72	64
OIKG(Ours)	11.58	2.18	81	76	12.37	2.68	75	65	13.40	3.05	74	64

TABLE II
EVALUATION RESULTS ON RXR DATASET UNDER DIFFERENT SETTINGS.
BEST PERFORMANCE IS HIGHLIGHTED IN BOLD.

Methods	Val Seen				Val Unseen			
	NE↓	SR↑	nDTW↑	sDTW↑	NE↓	SR↑	nDTW↑	sDTW↑
LSTM [9]	10.7	25.2	42.2	20.7	10.9	22.8	38.9	18.2
EnvDrop+ [52]	-	-	-	-	43.6	55.7	-	-
HAMT [30]	-	59.4	65.3	50.9	-	56.5	63.1	48.3
EnvEdit [32]	-	67.2	71.1	58.5	-	62.8	68.5	54.6
MPM [53]	-	67.7	71.0	58.9	-	63.5	67.7	54.5
MARVEL [54]	3.0	75.9	79.1	68.8	4.5	64.8	70.8	57.5
BEVBert [17]	3.2	75.0	76.3	66.7	4.0	68.5	69.6	58.6
PRET [18]	2.4	79.3	80.4	70.7	3.2	72.8	73.4	62.4
OIKG(Ours)	1.9	83.3	84.0	75.8	2.8	74.7	74.8	64.2

present a unified theoretical analysis covering both components: (i) decoupling angular–visual observation features with geometric embedding on directed edges, and (ii) extracting fine-grained location and object cues for instruction alignment. Taken together, Theorem 1 and Theorem 2 establish that reducing representational interference in spatial features and injecting explicit semantic detail from instructions jointly lower optimization variance, strengthen directional consistency, and increase semantic matching with true trajectories during training.

Definition 1 (Observation Feature Decoupling). *Let $F_o \in \mathbb{R}^{K \times D}$ be the observation feature matrix with K viewpoints and feature dimension D . Assume*

$$F_o = [A, V], \quad A \in \mathbb{R}^{K \times D_a}, \quad V \in \mathbb{R}^{K \times D_v}, \quad D_a + D_v = D. \quad (7)$$

Define the angular and visual embedding maps

$$E_a = \phi_a(A), \quad E_v = \phi_v(V), \quad (8)$$

where $\phi_a : \mathbb{R}^{D_a} \rightarrow \mathbb{R}^{D_e}$ and $\phi_v : \mathbb{R}^{D_v} \rightarrow \mathbb{R}^{D_e}$ are fully connected layers with ReLU activation. The fused observation embedding is

$$F'_o = \mathcal{F}([E_a, E_v]) = \text{MLP}([E_a, E_v]). \quad (9)$$

Definition 2 (Angular Distance Embedding). *Let $F_g \in \mathbb{R}^{N \times D_g}$ denote graph features with node angles $\alpha \in [0, 2\pi]^N$.*

Define

$$d_{ij} = \min_{k \in \mathbb{Z}} |\alpha_i - \alpha'_j + 2k\pi|. \quad (10)$$

The angular distance d_{ij} represents the minimum circular angle displacement between viewpoints i and j .

Definition 3 (Geometric Positional Embedding). *With d_{ij} defined in Definition 2 and based on Equation (3), define the geometric embedding*

$$\psi(\alpha_i, \alpha'_j) = \mathcal{P}(d_{ij}, \sin(\alpha_i - \alpha'_j), \cos(\alpha_i - \alpha'_j)), \quad (11)$$

and positional embedding

$$pe_{ij} = \psi(\alpha_i, \alpha'_j). \quad (12)$$

The updated graph embedding in Equation (4) is

$$F'_g = \mathcal{C}(\sin(\alpha), \cos(\alpha)) + pe. \quad (13)$$

Theorem 1 (Effectiveness of Decoupling and Geometric Embedding). *Let F'_o and F'_g be as defined in Definition 1, Definition 2, and Definition 3. Consider the navigation loss \mathcal{L} jointly optimized with respect to F'_o and F'_g . Then*

$$\mathbb{E}(\|\nabla_{F'_o, F'_g} \mathcal{L}\|^2) \leq \mathbb{E}(\|\nabla_{F_o, F_g} \mathcal{L}\|^2) - \delta, \quad (14)$$

for some constant $\delta > 0$, where the expectation is taken over the training data distribution.

Theorem 1 establishes that the joint effect of angular-visual decoupling and geometric embedding yields a strictly smaller expected gradient second moment than the coupled baseline. In other words, eliminating mixed-channel interference and providing explicit directional priors decreases gradient variance, improves conditioning of the optimization landscape, and enhances convergence rate in learning navigable edge relationships.

This theoretical result aligns with our empirical findings on R2R and RxR benchmarks, where OIKG consistently improves success-related metrics and trajectory alignment scores. By enforcing disentangled representations and introducing angular continuity into graph edges, the training process becomes smoother, less volatile, and more capable of constructing accurate directional paths. A complete proof of Theorem 1 and its derivations is provided in the Supplementary material I.

Building on the optimization stability and gradient variance reduction established in Theorem 1, we now analyze the second core design of OIKG: the key-detail guidance mechanism. While the previous theorem explains why spatial interaction becomes more stable during learning, the following result demonstrates how separating location-critical and object-critical textual cues further improves semantic correspondence between instructions and navigable graph structures.

Theorem 2 (Fine-Grained Information Gain and Alignment Accuracy of the Key-Detail Guidance Module). *Let the natural language instruction I be encoded by a pre-trained language model into a feature sequence $F_i \in \mathbb{R}^{M \times D_t}$, where M is the number of tokens and D_t is the text feature dimension. Assume there exist two learnable linear projectors $\mathcal{E}_{\mathcal{L}}$ and $\mathcal{E}_{\mathcal{O}}$ that extract location detail features $F_{\mathcal{L}} \in \mathbb{R}^{D_k}$ and object detail features $F_{\mathcal{O}} \in \mathbb{R}^{D_k}$ from F_i , respectively. These are fused to obtain a key detail feature*

$$F_k = \mathcal{F}'([F_{\mathcal{L}}, F_{\mathcal{O}}]) \in \mathbb{R}^{D_k}. \quad (15)$$

Let the cross-modal feature $F_c \in \mathbb{R}^{N \times D_c}$ be the fused representation of graph features and instruction features, where N is the number of nodes. Define the fine-grained alignment function

$$\text{Align}(F_c, F_k) = \text{Softmax}\left(\frac{F_c W_q (F_k W_k)^T}{\sqrt{d}}\right) F_k W_v, \quad (16)$$

where $W_q, W_k, W_v \in \mathbb{R}^{D_c \times d}$ are learnable weight matrices and d is the attention dimension. When key-detail guidance is applied, the aligned feature is

$$F_e = F_c + \text{Align}(F_c, F_k). \quad (17)$$

Then the semantic matching score between F_e and the ground-truth navigation path graph G_{gt} satisfies

$$S(F_e, G_{gt}) - S(F_c, G_{gt}) \geq \rho \cdot MI(F_{\mathcal{L}}; G_{gt}) + \rho \cdot MI(F_{\mathcal{O}}; G_{gt}), \quad (18)$$

for some constant $\rho > 0$ that depends on model capacity, where $MI(\cdot; \cdot)$ denotes mutual information.

A full derivation and proof of Theorem 2 are provided in the Supplementary material II. Theorem 2 shows that extracting location-oriented and object-oriented components from raw instructions increases mutual information with the true navigation trajectory. By isolating two classes of instruction cues that directly govern movement decisions—where to go and what to find—our method raises alignment accuracy and strengthens cross-modal fusion beyond conventional attention-based instruction conditioning. The improvement is reflected in better semantic scoring against reference routes and more reliable decision-making in long-range multi-step planning. Together with Theorem 1, this result provides a joint theoretical justification that OIKG both stabilizes directional feature learning and enhances instruction-level specificity, enabling more accurate and consistent navigation behavior.

V. EXPERIMENTS

A. Implementation Details

We implement the proposed method using PyTorch [55] and conduct all experiments on a single NVIDIA A6000 GPU. Model optimization is performed using the AdamW [56] optimizer. During the pretraining stage, the learning rate is set to 2e-5, the batch size is 16, and training is carried out for 100,000 iterations. For task-specific fine-tuning, the learning rate is reduced to 1e-5, the batch size is set to 8, and the model is trained for 200,000 iterations. The weighting coefficient λ in the loss function is fixed to 0.2 across all experiments.

For both the R2R and RxR datasets, we adopt augmented training data provided by prior works to improve generalization performance. Unless otherwise specified, all reported results are obtained using the same network architecture and training protocol, ensuring fair comparisons with existing methods [37], [54].

B. Comparison on R2R Dataset

1) *R2R Dataset*: The Room-to-Room (R2R) [8] dataset consists of 7,189 navigation trajectories collected from 90 indoor scenes, with each trajectory paired with three natural language instructions. The environments are represented by panoramic viewpoints, where each viewpoint comprises 36 discretized visual observations. The dataset is divided into training, validation seen, validation unseen, and test unseen splits. The validation seen split shares the same environments as the training set, while the validation unseen and test unseen splits evaluate generalization to novel scenes. All trajectories in R2R correspond to shortest paths between the start and target locations.

2) *Evaluation Metrics*: Following standard evaluation protocols [17], [18], we report four metrics to assess navigation performance. (a) Trajectory Length (*TL*) measures the average length of the executed navigation paths. (b) Navigation Error (*NE*) denotes the mean shortest-path distance between the agent’s final position and the target location. (c) Success Rate (*SR*) represents the percentage of episodes in which the agent terminates within 3 meters of the target. (d) Success weighted by Path Length (*SPL*) further accounts for navigation efficiency by balancing success rate against trajectory length, with higher values indicating more effective navigation.

Leave the room and take a **right**. Walk pass the **stairs** and enter the bedroom on the **right**. Stop once you pass the **door** to the **bedroom**.



Fig. 3. Qualitative results on the R2R Dataset. The green box indicates the location details, and the blue box represents the object details.

3) *Quantitative Results*: We compare the proposed method with a wide range of representative VLN approaches, including Seq2Seq-SF [8], Speaker-Follower [28], RCM [29], Regretful [49], EnvDrop [31], PREVALENT [37], NvEM [50], SSM [46], RecBert [51], HAMT [30], MTVM [38], DUET [13], AZHP [14], Meta-Explore [15], GridMM [16], BEVBert [17] and PRET [18]. Quantitative results on the R2R benchmark are summarized in Table I. The proposed method achieves competitive or superior performance across different evaluation splits, with particularly strong results on the SPL metric, which reflects both navigation accuracy and efficiency. These results indicate that fine-grained instruction-guided graph reasoning improves the agent's ability to follow navigation instructions while maintaining efficient trajectories.

In addition to quantitative evaluation, qualitative examples are presented in Fig. 3, illustrating that the proposed method is able to accurately interpret instructions and generate coherent navigation trajectories in complex indoor environments.

C. Comparison on RxR Dataset

1) *RxR Dataset*: The Room-across-Room (RxR) [9] dataset is a large-scale multilingual benchmark for VLN. It contains a total of 126,000 navigation instructions evenly distributed across three languages: English, Hindi, and Telugu. Compared with R2R, navigation trajectories in RxR are substantially longer and do not necessarily correspond to shortest paths. Moreover, RxR instructions are more descriptive and linguistically complex, posing additional challenges for long-horizon reasoning and fine-grained instruction understanding.

2) *Evaluation Metrics*: Due to the non-shortest-path nature of trajectories in RxR, trajectory length-based metrics such as TL and SPL are not applicable. Following established evaluation protocols [17], [18], we report four metrics: Navigation Error (NE), Success Rate (SR), Normalized Dynamic Time Warping ($nDTW$), and Success weighted Dynamic Time Warping ($sDTW$). Among these, $nDTW$ measures the similarity between the predicted and ground-truth trajectories, while $sDTW$ further incorporates task success, providing a comprehensive assessment of trajectory alignment quality.

3) *Quantitative Results*: We compare the proposed method with several representative baselines, including LSTM-based models [9], EnvDrop+ [52], HAMT [30], EnvEdit [32], MPM [53], MARVEL [54], BEVBert [17], and PRET [18].

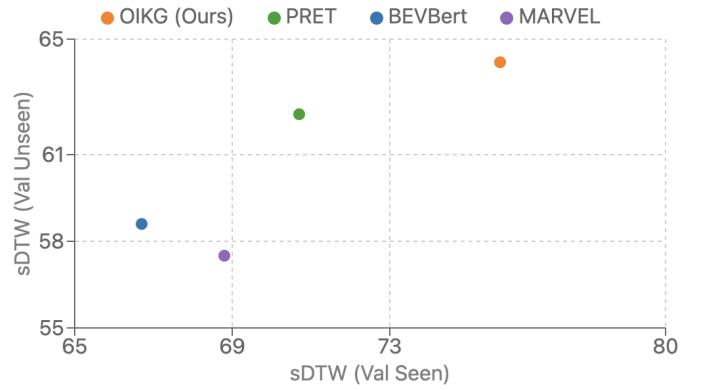


Fig. 4. Comparison of sDTW on the RxR val seen split and the RxR val unseen split. OIKG demonstrates the ability to achieve optimal sDTW across various splits.

Quantitative results on the RxR benchmark are reported in Table II. As illustrated in Fig. 4, the proposed method achieves the best performance across all evaluation metrics on both validation seen and validation unseen splits. In particular, consistent improvements in $nDTW$ and $sDTW$ indicate more accurate trajectory alignment and stronger instruction-following capability, especially in challenging unseen environments. These results demonstrate that fine-grained instruction-guided graph reasoning effectively enhances navigation robustness under long and linguistically complex instructions.

D. Ablation Study

To analyze the contribution of each component in the proposed framework, we conduct ablation experiments on the R2R validation unseen split. The results are summarized in Table III, where different model variants are evaluated by selectively removing or adding individual components. All ablation models are trained and evaluated under the same experimental settings to ensure fair comparisons.

We first examine the impact of the multi-element decoupling (MED) mechanism, which separates angular and visual information within observation features. As shown in Table III (Row 2), incorporating MED leads to consistent improvements over the baseline across all evaluation metrics. This observation suggests that mitigating representational interference between heterogeneous observation cues facilitates more accurate spatial reasoning during navigation.

TABLE III
ABLATION STUDIES OF EACH COMPONENT.

#	MED	GE	LD	OD	TL	NE↓	SR↑	SPL↑	time(ms)↓
1	-	-	-	-	12.59	3.01	73.32	63.07	3.69
2	✓	-	-	-	12.72	2.97	74.13	63.48	3.75
3	✓	✓	-	-	12.41	2.85	74.70	63.72	3.80
4	✓	✓	✓	-	12.30	2.84	74.78	64.24	3.97
5	✓	✓	✓	✓	12.37	2.68	75.54	65.60	4.08

Next, we evaluate the effect of the geometric embedding (GE) module, which enhances directed edge representations by explicitly modeling relative angular relationships. Comparing Rows 2 and 3 in Table III, the inclusion of GE further improves navigation performance, particularly in terms of NE and SR. These results indicate that geometric priors provide useful directional information that strengthens the expressiveness of the navigation graph.

We further investigate the contribution of fine-grained instruction modeling by incrementally introducing location details (LD) and object details (OD). As shown in Rows 4 and 5, adding location-specific cues improves the agent's ability to identify relevant spatial regions, while incorporating object-centric cues yields additional gains in success-related metrics. The combined use of LD and OD achieves the best overall performance, highlighting the complementary roles of spatial and object-level semantics in instruction understanding.

Finally, we analyze the computational overhead introduced by the additional components. The inference time reported in Table III shows that the proposed modules incur only a marginal increase in runtime, demonstrating that the performance gains are achieved without a significant compromise in computational efficiency. Overall, the ablation results confirm that each component of the proposed framework contributes meaningfully to navigation performance and that their combination yields the most effective and robust behavior.

VI. CONCLUSION

In this paper, we presented a fine-grained instruction-guided graph reasoning framework for Vision-and-Language Navigation. The proposed approach enhances spatial reasoning by explicitly modeling observation-graph interactions and reducing representational interference between angular and visual cues, while simultaneously improving instruction following through fine-grained modeling of location-specific and object-centric semantics. By jointly strengthening structured graph representations and instruction-level semantic alignment, the proposed method enables more accurate and robust navigation behavior in complex environments. Extensive evaluations on the R2R and RxR benchmarks demonstrate that the proposed framework consistently outperforms existing state-of-the-art approaches across multiple metrics, particularly in challenging unseen environments. In addition, ablation studies and theoretical analysis validate the effectiveness of each core component and provide insights into why fine-grained instruction-guided graph reasoning improves navigation performance. Despite the promising results, some limitations remain. First, the proposed method relies on pre-defined location and object vocabularies

extracted offline, which may not generalize to instructions with novel terminology. Second, the current framework is evaluated only in simulation environments; transferring to real-world robotic systems with noisy observations remains an open challenge. Future work will explore adaptive vocabulary learning to improve generalization to diverse linguistic expressions, extending the proposed framework to continuous navigation settings, and incorporating more expressive multimodal representations to further enhance scalability in real-world embodied navigation scenarios.

REFERENCES

- [1] J. Gu, E. Stefani, Q. Wu, J. Thomason, and X. Wang, "Vision-and-language navigation: A survey of tasks, methods, and future directions," in *Proceedings of the 60th Annual Meeting of the Association for Computational Linguistics (Volume 1: Long Papers)*, pp. 7606–7623, 2022.
- [2] B. Lin, Y. Nie, Z. Wei, J. Chen, S. Ma, J. Han, H. Xu, X. Chang, and X. Liang, "Navcot: Boosting llm-based vision-and-language navigation via learning disentangled reasoning," *IEEE Transactions on Pattern Analysis and Machine Intelligence*, 2025.
- [3] T. Yu, Y. Wu, Q. Cui, Q. Huang, and J. Yu, "Mossvln: Memory-observation synergistic system for continuous vision-language navigation," *IEEE Transactions on Multimedia*, 2025.
- [4] K. Chen, D. An, Y. Huang, R. Xu, Y. Su, Y. Ling, I. Reid, and L. Wang, "Constraint-aware zero-shot vision-language navigation in continuous environments," *IEEE Transactions on Pattern Analysis and Machine Intelligence*, 2025.
- [5] S. Wen, Z. Zhang, Y. Sun, and Z. Wang, "Ovl-map: An online visual language map approach for vision-and-language navigation in continuous environments," *IEEE Robotics and Automation Letters*, 2025.
- [6] R. Liu, W. Wang, and Y. Yang, "Volumetric environment representation for vision-language navigation," in *Proceedings of the IEEE/CVF conference on computer vision and pattern recognition*, pp. 16317–16328, 2024.
- [7] S. Wu, X. Fu, F. Wu, and Z.-J. Zha, "Vision-and-language navigation via latent semantic alignment learning," *IEEE Transactions on Multimedia*, vol. 26, pp. 8406–8418, 2024.
- [8] P. Anderson, Q. Wu, D. Teney, J. Bruce, M. Johnson, N. Sünderhauf, I. Reid, S. Gould, and A. Van Den Hengel, "Vision-and-language navigation: Interpreting visually-grounded navigation instructions in real environments," in *Proceedings of the IEEE Conference on Computer Vision and Pattern Recognition*, pp. 3674–3683, 2018.
- [9] A. Ku, P. Anderson, R. Patel, E. Ie, and J. Baldridge, "Room-across-room: Multilingual vision-and-language navigation with dense spatiotemporal grounding," in *Proceedings of the 2020 Conference on Empirical Methods in Natural Language Processing (EMNLP)*, pp. 4392–4412, 2020.
- [10] S. Wang, Z. Wu, X. Hu, Y. Lin, and K. Lv, "Skill-based hierarchical reinforcement learning for target visual navigation," *IEEE Transactions on Multimedia*, vol. 25, pp. 8920–8932, 2023.
- [11] Y. Qiao, Y. Qi, Y. Hong, Z. Yu, P. Wang, and Q. Wu, "Hop+: History-enhanced and order-aware pre-training for vision-and-language navigation," *IEEE Transactions on Pattern Analysis and Machine Intelligence*, vol. 45, no. 7, pp. 8524–8537, 2023.
- [12] R. Liu, X. Wang, W. Wang, and Y. Yang, "Bird's-eye-view scene graph for vision-language navigation," in *Proceedings of the IEEE/CVF International Conference on Computer Vision*, pp. 10968–10980, 2023.
- [13] S. Chen, P.-L. Guhur, M. Tapaswi, C. Schmid, and I. Laptev, "Think global, act local: Dual-scale graph transformer for vision-and-language navigation," in *Proceedings of the IEEE/CVF Conference on Computer Vision and Pattern Recognition*, pp. 16537–16547, 2022.
- [14] C. Gao, X. Peng, M. Yan, H. Wang, L. Yang, H. Ren, H. Li, and S. Liu, "Adaptive zone-aware hierarchical planner for vision-language navigation," in *Proceedings of the IEEE/CVF Conference on Computer Vision and Pattern Recognition*, pp. 14911–14920, 2023.
- [15] M. Hwang, J. Jeong, M. Kim, Y. Oh, and S. Oh, "Meta-explore: Exploratory hierarchical vision-and-language navigation using scene object spectrum grounding," in *Proceedings of the IEEE/CVF Conference on Computer Vision and Pattern Recognition*, pp. 6683–6693, 2023.

[16] Z. Wang, X. Li, J. Yang, Y. Liu, and S. Jiang, "Gridmm: Grid memory map for vision-and-language navigation," in *Proceedings of the IEEE/CVF International Conference on Computer Vision*, pp. 15625–15636, 2023.

[17] D. An, Y. Qi, Y. Li, Y. Huang, L. Wang, T. Tan, and J. Shao, "Bevbert: Multimodal map pre-training for language-guided navigation," in *Proceedings of the IEEE/CVF International Conference on Computer Vision*, pp. 2737–2748, 2023.

[18] R. Lu, J. Meng, and W.-S. Zheng, "Pret: Planning with directed fidelity trajectory for vision and language navigation," in *European Conference on Computer Vision*, pp. 72–88, Springer, 2024.

[19] A. Radford, J. W. Kim, C. Hallacy, A. Ramesh, G. Goh, S. Agarwal, G. Sastry, A. Askell, P. Mishkin, J. Clark, *et al.*, "Learning transferable visual models from natural language supervision," in *International conference on machine learning*, pp. 8748–8763, PMLR, 2021.

[20] M. Oquab, T. Dariseti, T. Moutakanni, H. Vo, M. Szafraniec, V. Khalidov, P. Fernandez, D. Haziza, F. Massa, A. El-Nouby, *et al.*, "Dinov2: Learning robust visual features without supervision," *Transactions on Machine Learning Research Journal*, pp. 1–31, 2024.

[21] X. Li, Z. Wang, J. Yang, Y. Wang, and S. Jiang, "Kerm: Knowledge enhanced reasoning for vision-and-language navigation," in *Proceedings of the IEEE/CVF Conference on Computer Vision and Pattern Recognition*, pp. 2583–2592, 2023.

[22] X. Wang, W. Wang, J. Shao, and Y. Yang, "Lana: A language-capable navigator for instruction following and generation," in *Proceedings of the IEEE/CVF conference on computer vision and pattern recognition*, pp. 19048–19058, 2023.

[23] J. Li, R. Selvaraju, A. Gotmare, S. Joty, C. Xiong, and S. C. H. Hoi, "Align before fuse: Vision and language representation learning with momentum distillation," *Advances in Neural Information Processing Systems*, vol. 34, pp. 9694–9705, 2021.

[24] A. Conneau, "Unsupervised cross-lingual representation learning at scale," *arXiv preprint arXiv:1911.02116*, 2019.

[25] J. Li and M. Bansal, "Improving vision-and-language navigation by generating future-view image semantics," in *Proceedings of the IEEE/CVF conference on computer vision and pattern recognition*, pp. 10803–10812, 2023.

[26] K. Lin, P. Chen, D. Huang, T. H. Li, M. Tan, and C. Gan, "Learning vision-and-language navigation from youtube videos," in *Proceedings of the IEEE/CVF International Conference on Computer Vision*, pp. 8317–8326, 2023.

[27] Y. X. B. O. F. M. Y. Liu, "Observation-graph interaction and key-detail guidance for vision and language navigation," in *IEEE/RSJ International Conference on Intelligent Robots and Systems (IROS)*, pp. 15306–15313, 2025.

[28] D. Fried, R. Hu, V. Cirik, A. Rohrbach, J. Andreas, L.-P. Morency, T. Berg-Kirkpatrick, K. Saenko, D. Klein, and T. Darrell, "Speaker-follower models for vision-and-language navigation," *Advances in neural information processing systems*, vol. 31, 2018.

[29] X. Wang, Q. Huang, A. Celikyilmaz, J. Gao, D. Shen, Y.-F. Wang, W. Y. Wang, and L. Zhang, "Reinforced cross-modal matching and self-supervised imitation learning for vision-language navigation," in *Proceedings of the IEEE/CVF conference on computer vision and pattern recognition*, pp. 6629–6638, 2019.

[30] S. Chen, P.-L. Guhur, C. Schmid, and I. Laptev, "History aware multimodal transformer for vision-and-language navigation," *Advances in neural information processing systems*, vol. 34, pp. 5834–5847, 2021.

[31] H. Tan, L. Yu, and M. Bansal, "Learning to navigate unseen environments: Back translation with environmental dropout," in *Proceedings of the 2019 Conference of the North American Chapter of the Association for Computational Linguistics: Human Language Technologies, Volume 1 (Long and Short Papers)*, pp. 2610–2621, 2019.

[32] J. Li, H. Tan, and M. Bansal, "Enedit: Environment editing for vision-and-language navigation," in *Proceedings of the IEEE/CVF Conference on Computer Vision and Pattern Recognition*, pp. 15407–15417, 2022.

[33] C. Liu, F. Zhu, X. Chang, X. Liang, Z. Ge, and Y.-D. Shen, "Vision-language navigation with random environmental mixup," in *Proceedings of the IEEE/CVF International Conference on Computer Vision*, pp. 1644–1654, 2021.

[34] A. Vaswani, "Attention is all you need," *Advances in Neural Information Processing Systems*, 2017.

[35] Y. Xie, J. Zhu, S. Li, and P. Shi, "Cross-modal information-guided network using contrastive learning for point cloud registration," *IEEE Robotics and Automation Letters*, vol. 9, no. 1, pp. 103–110, 2023.

[36] Y. Xie, T. Feng, X. Zhang, X. Luo, Z. Guo, W. Yu, H. Chang, F. Ma, and F. R. Yu, "Pointtalk: Audio-driven dynamic lip point cloud for 3d gaussian-based talking head synthesis," *arXiv preprint arXiv:2412.08504*, 2024.

[37] W. Hao, C. Li, X. Li, L. Carin, and J. Gao, "Towards learning a generic agent for vision-and-language navigation via pre-training," in *Proceedings of the IEEE/CVF Conference on Computer Vision and Pattern Recognition*, pp. 13137–13146, 2020.

[38] C. Lin, Y. Jiang, J. Cai, L. Qu, G. Haffari, and Z. Yuan, "Multimodal transformer with variable-length memory for vision-and-language navigation," in *European Conference on Computer Vision*, pp. 380–397, Springer, 2022.

[39] J. Fuentes-Pacheco, J. Ruiz-Ascencio, and J. M. Rendón-Mancha, "Visual simultaneous localization and mapping: a survey," *Artificial intelligence review*, vol. 43, pp. 55–81, 2015.

[40] Y. Wang, Y. Tian, J. Chen, K. Xu, and X. Ding, "A survey of visual slam in dynamic environment: the evolution from geometric to semantic approaches," *IEEE Transactions on Instrumentation and Measurement*, 2024.

[41] D. S. Chaplot, D. P. Gandhi, A. Gupta, and R. R. Salakhutdinov, "Object goal navigation using goal-oriented semantic exploration," *Advances in Neural Information Processing Systems*, vol. 33, pp. 4247–4258, 2020.

[42] J. F. Henriques and A. Vedaldi, "Mapnet: An allocentric spatial memory for mapping environments," in *proceedings of the IEEE Conference on Computer Vision and Pattern Recognition*, pp. 8476–8484, 2018.

[43] Y. Xie, J. Zhu, S. Li, N. Hu, and P. Shi, "Hecpg: Hyperbolic embedding and confident patch-guided network for point cloud matching," *IEEE Transactions on Geoscience and Remote Sensing*, 2024.

[44] D. S. Chaplot, R. Salakhutdinov, A. Gupta, and S. Gupta, "Neural topological slam for visual navigation," in *Proceedings of the IEEE/CVF conference on computer vision and pattern recognition*, pp. 12875–12884, 2020.

[45] K. Chen, J. K. Chen, J. Chuang, M. Vázquez, and S. Savarese, "Topological planning with transformers for vision-and-language navigation," in *Proceedings of the IEEE/CVF Conference on Computer Vision and Pattern Recognition*, pp. 11276–11286, 2021.

[46] H. Wang, W. Wang, W. Liang, C. Xiong, and J. Shen, "Structured scene memory for vision-language navigation," in *Proceedings of the IEEE/CVF conference on Computer Vision and Pattern Recognition*, pp. 8455–8464, 2021.

[47] A. Chang, A. Dai, T. Funkhouser, M. Halber, M. Niebner, M. Savva, S. Song, A. Zeng, and Y. Zhang, "Matterport3d: Learning from rgb-d data in indoor environments," in *International Conference on 3D Vision (3DV)*, 2017.

[48] D. An, H. Wang, W. Wang, Z. Wang, Y. Huang, K. He, and L. Wang, "Etpnav: Evolving topological planning for vision-language navigation in continuous environments," *IEEE Transactions on Pattern Analysis and Machine Intelligence*, 2024.

[49] C.-Y. Ma, Z. Wu, G. AlRegib, C. Xiong, and Z. Kira, "The regretful agent: Heuristic-aided navigation through progress estimation," in *Proceedings of the IEEE/CVF conference on Computer Vision and Pattern Recognition*, pp. 6732–6740, 2019.

[50] D. An, Y. Qi, Y. Huang, Q. Wu, L. Wang, and T. Tan, "Neighbor-view enhanced model for vision and language navigation," in *Proceedings of the 29th ACM International Conference on Multimedia*, pp. 5101–5109, 2021.

[51] Y. Hong, Q. Wu, Y. Qi, C. Rodriguez-Opazo, and S. Gould, "Vln bert: A recurrent vision-and-language bert for navigation," in *Proceedings of the IEEE/CVF conference on Computer Vision and Pattern Recognition*, pp. 1643–1653, 2021.

[52] S. Shen, L. H. Li, H. Tan, M. Bansal, A. Rohrbach, K.-W. Chang, Z. Yao, and K. Keutzer, "How much can clip benefit vision-and-language tasks?"

[53] Z.-Y. Dou, F. Gao, and N. Peng, "Masked path modeling for vision-and-language navigation."

[54] S. Wang, C. Montgomery, J. Orbay, V. Birodkar, A. Faust, I. Gur, N. Jaques, A. Waters, J. Baldridge, and P. Anderson, "Less is more: Generating grounded navigation instructions from landmarks," in *Proceedings of the IEEE/CVF Conference on Computer Vision and Pattern Recognition*, pp. 15428–15438, 2022.

[55] A. Paszke, S. Gross, F. Massa, A. Lerer, J. Bradbury, G. Chanan, T. Killeen, Z. Lin, N. Gimelshein, L. Antiga, *et al.*, "Pytorch: An imperative style, high-performance deep learning library," *Advances in Neural Information Processing Systems*, vol. 32, 2019.

[56] I. Loshchilov, "Decoupled weight decay regularization," *arXiv preprint arXiv:1711.05101*, 2017.